Clinical Case Report

Medicine®

OPEN

A highly malignant case of neuroblastoma with substantial increase of single-nucleotide variants and normal mismatch repair system

A case report

Lin-Qing Yuan, MD[a], Jin-Hu Wang, MD[a], Kun Zhu, MD[a], Min Yang, MD[a], Wei-Zhong Gu, MD[a,c], Can Lai, MD[a], Hao-Min Li, PhD[b,c], Qiang Shu, MD, PhD[c], Xi Chen, MD, PhD[a,c,*]

Abstract

Rationale: Neuroblastoma is a common abdominal malignancy in children. The chemoresistant and relapsed cases have poor prognosis. The genetic background and the mechanism of resistance remain unelucidated. Next-generation sequence (NGS) is becoming a popular tool to unravel the genetic background and to guide precision medicine in oncology studies as well as in clinical practice.

Patient concerns: Here we report a neuroblastoma case of a boy aged 2 years and 8 months when first diagnosed, with multiple metastatic sites found in both lungs. The metastatic tumors were resistant to chemotherapy and the patient suffered from severe bone marrow suppression. NGS of the whole exon revealed somatic mutations including 9666 single-nucleotide variants (SNVs) from 5148 genes, 55 copy number variations (CNVs), and 140 insertion–deletion variations. The high frequency of SNVs makes it distinguished case. However, no mutation of key tumor driver genes with functional significance was identified. No abnormality was found in nucleic acid synthesis enzymes. No amplification of *c-Myc* and *n-Myc* was found by fluorescence in situ hybridization (FISH). Both NGS and immunohistochemistry (IHC) analysis indicated that DNA mismatch repair (MMR) system was intact.

Interventions: After initial diagnosis, the patient received combinational chemotherapy, which includes vindesine, an analogue of adriamycin suggested by NGS data, for 4 months. Radical section of the tumor together with the left kidney and the left adrenal gland was performed 5 months after diagnosis. Postsurgical chemotherapy protocols was similar with the previous.

Outcomes: The patient died 2 years after initial diagnosis after 8 relapses following combinational chemotherapy.

Lessons: This case of neuroblastoma is with pronounced somatic mutations but unidentified driver gene and therapeutic target. Although NGS is a potentially powerful tool to guide precision medicine, at current stage, its application in the clinic certainly has its limits. The underlying mechanism of the substantially increased SNV number, as well as the malignant behaviors of the tumor, is yet to be revealed.

Abbreviations: ACEI = angiotension-converting enzyme inhibitors, ALK = anaplastic lymphoma kinase, CDS = coding sequence, CMMRD = constitutional DNA mismatch repair deficiency, CNV = copy number variation, CT = computed tomography, EGFR = epidermal growth factor receptor, EMA = epithelial membrane antigen, ENQUA = European neuroblastoma quality assessment, FISH = fluorescence in situ hybridization, HE = hematoxylin and eosin, hMLH = human MutL homologs, hMSH = human MutS homologs, IHC = immunohistochemistry, INDEL = insertion–deletion variation, INSS = neuroblastoma staging system, MDR = multiple drug resistance, MMR = DNA mismatch repair, ncRNA = noncoding RNA, NGS = next generation sequencing, SNP = single-nucleotide polymorphism, SNV = single-nucleotide variant, SYN = synapsin, TSS = transcription start site, TTS = transcription termination site, UTR = untranslated region, WT1 = Wilms' tumor 1.

Keywords: DNA mismatch repair, Myc, multiple drug resistance, neuroblastoma, next-generation sequencing, precision medicine, somatic mutation

Editor: N/A.

L-QY and J-HW contributed equally to this study.

All authors certify that they have no affiliations with or involvement in any organization or entity with any financial interest (such as honoraria; educational grants; participation in speakers' bureaus; membership, employment, consultancies, stock ownership, or other equity interest; and expert testimony or patent-licensing arrangements), or nonfinancial interest (such as personal or professional relationships, affiliations, knowledge, or beliefs) in the subject matter or materials discussed in this manuscript.

This research is supported by National Science Foundation of Zhejiang Province, China (LY15H160024) and National Science Foundation of China (No. 81202021).

The authors have no conflicts of interest to disclose.

[a] Departments of Central Laboratory, Pathology, Oncology and Radiology, The Children's Hospital of Zhejiang University School of Medicine, [b] Institute of Translational Medicine, Zhejiang University, [c] The Key Laboratory of Diagnosis and Treatment of Neonatal Diseases of Zhejiang Province, Hangzhou, Zhejiang, China.

[*] Correspondence: Xi Chen, The Children's Hospital of Zhejiang University School of Medicine, No. 3333 Binsheng Road, Hangzhou 310052, Zhejiang Province, China (e-mail: chchenxi@zju.edu.cn).

Medicine (2017) 96:50(e8845)

Received: 26 August 2017 / Received in final form: 29 October 2017 / Accepted: 2 November 2017

http://dx.doi.org/10.1097/MD.0000000000008845

1. Introduction

Neuroblastoma is a common abdominal malignancy in children with relatively poor prognosis compared with other childhood tumors. Choice of treatment procedure is made according to the risk stratification based on clinical manifestations and the pathological type. In the international neuroblastoma staging system (INSS) commonly used in the clinic,[1] any primary tumor with dissemination to distant organs is defined as stage IV that requires chemotherapy before and after radical surgery. Common migration sites include the lymph nodes, bone marrow, bone, liver, and skin. Metastasis of neuroblastoma to the lung is rare, with a reported occurrence rate of 3% to 4%,[2] and diffused dissemination to the lung is extremely rare.

The histological manifestation of neuroblastoma is highly heterogeneous. Its mutational dynamics is to be investigated for the practice of precision medicine. Up to now, only a few studies using next-generation sequencing (NGS) to analyze the genetic background of neuroblastoma have been reported.[3–9] However, the paradigm of classical driver genes including *MYC*, *RAS*, and *ALK* has not been shifted, and not much progress has been made in discovery of applicable therapeutic targets.

The DNA mismatch repair (MMR) system is a mechanism for genome maintenance. The system is composed of proteins that can recognize and degrade one strand of DNA and use the complementary strand as a repair template to eliminate the mismatch.[10] The MMR system in human is composed of 6 proteins: hMSH2, hMSH3, hMSH6, hMLH1, hMLH3, and hPMS1. Defect of the MMR system substantially elevates spontaneous mutation rates. In pediatrics, constitutional MMR deficiency (CMMRD) syndrome is resulted from biallelic germline loss-of-function mutations in one of the MMR genes. Individuals with CMMRD have a high risk to develop a broad spectrum of malignancies, including high-grade glioma, acute myeloid leukemia, or rhabdomyosarcoma.[11] MMR deficiency was found first to contribute to colorectal cancer,[12] later in many other types of cancers, and this pathological condition has been named as Lynch syndrome that is replacing the definition of CMMRD.[13] In pediatric neuroblastoma, analysis of MMR proteins expression levels has been reported.[14] In cultured neuroblastoma cells, MMR deficiency contributes to the malignant behaviors such as colony formation.[15] In this case report, a highly malignant neuroblastoma with lung metastasis and multiple drug resistance (MDR) is reported. The genetics background was analyzed using NGS combined with traditional methods.

2. Materials and methods

2.1. Sample collection

This research was approved by the institutional ethical committee in 2014 and was done in accordance with the Helsinki Declaration of 1975. Signed informed consent forms were obtained from the patient's guardian. Tissue samples were taken after surgery. Neuroblastoma with poor differentiation was diagnosed by postsurgical pathological examinations. Whole blood with anticoagulant was also collected.

2.2. Whole exome sequencing

NGS was performed by Novogene, Beijing, China. Total DNA was extracted from the tissue and the blood. After building the DNA library, target exome sequences were captured by liquid-phase chips (Agilent) and were sequenced by NGS (Hiseq 2000; Illumina). Somatic SNV was analyzed by muTect (muTect-1.1.4.jar) and by COSMIC plus DBSNP online databases.

2.3. Pathological analysis

Tissues were fixed in 4% paraformaldehyde, embedded in paraffin and cut into 4 μm sections, then subjected to hematoxylin and eosin (HE) staining. Immunohistochemistry (IHC) analysis was performed by primary antibodies against hMSH2 and hMLH1 (Protein Tech) and with a biotinylated peroxidase-conjugated streptavidin system (Bio-Genex Laboratories). IHC of SYN, CD56, vimentin, CD99, Wilms' tumor 1 (WT1), epidermal growth factor receptor (EMA), and desmin (primary antibodies from Dako, Denmark) were also performed. All specimens were scanned by 3DHistech (Pannoramic, Hungary) with companion software.

2.4. Fluorescence in situ hybridization (FISH)

Amplification of *Myc* was detected by commercial kit (Vysis, Abbott) using fluorescent probe against the *c-Myc* and *n-Myc* genes in sectioned paraffin-embedded tissue. Based on the guidelines of European neuroblastoma quality assessment (ENQUA),[16] over 100 cells were counted. As the diagnostic criteria, samples with $<5\%$ cells with >4 probes bound to the chromosomes were considered negative.

3. Case report

3.1. Clinical data and treatment procedure

The patient was a boy aged 2 years and 8 months when first admitted to the hospital due to palpable left-side abdominal mass. Needle biopsy and pathological examinations diagnosed the patient as neuroblastoma with poor differentiation. No migration to the bone marrow was detected. Computed tomography (CT) revealed multiple migration loci in the lung and pleural fluid (Fig. 1A), but no migration to the liver or to the bone. The patient received chemotherapy for 4 months by

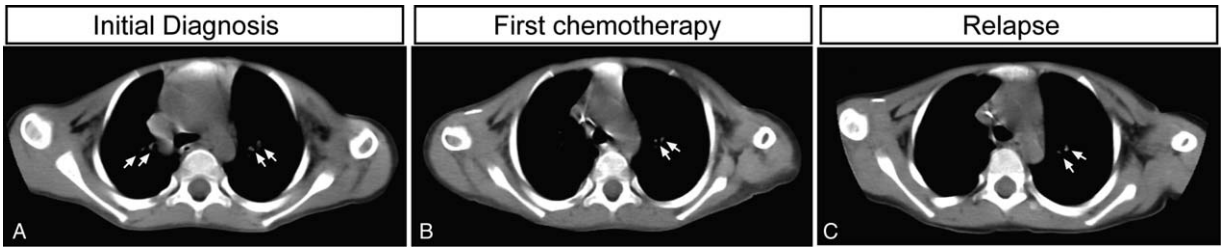

Figure 1. CT scans of the metastatic tumors in the lung. (A) Image of a representative window at primary diagnosis. (B) Image of the same window after chemotherapy and surgery. (C) Image of the same window in the follow-up examinations after tumor relapses. Arrows indicate the loci of the metastatic tumors.

combination of vindesine+ifosfamide+etoposide and vindesine +tsprubicine+carboplatin, topotecan, and gemcitabine were also used. Then radical section of the tumor together with the left kidney and the left adrenal gland was performed 5 months after diagnosis. Pathological examinations confirmed neuroblastoma with poor differentiation and massive necrosis. A later CT showed that after first session of chemotherapy, both the number and the size of the high-density loci in the lung were reduced (Fig. 1B). The patient received several postsurgical chemotherapy protocols similar with the previous. He was always developing severe bone marrow suppression upon chemotherapy with low white blood cell and platelet counts, and severe respiratory inflammation. Follow-up CT scans found no relapse of the original tumor in the adrenal gland, but multiple metastatic loci in both lungs, with new loci developed after surgery (Fig. 1C). No metastasis in other organs was detected. The patient died 22 months after diagnosis, 17 months after surgery. The timeline of the reported case from initial diagnosis to death is summarized in Table 1.

3.2. Pathology and FISH

In the tissue from needle biopsy of the mass from left kidney by HE staining (Fig. 2A), necrosis was commonly seen. Clusters of tumor cells with poor differentiation and with round nuclei could be observed; no anaplastic cells were observed; spindle-like fibers could be observed. The postsurgery specimen was the sectioned left kidney, left adrenal gland together with the tumor. The tumor was located above the kidney, with a size of $7 \times 6.5 \times 5$ cm and massive necrotic area of 5.5×5 cm. The tumor had invaded the envelope of the kidney, but not into the renal pelvis and the ureter. Blood congestion, edema, and partial hyaloid degeneration were observed in the fat and fibrous tissues surrounding the tumor mass. Postsurgical pathological examinations revealed similar cellular morphology with significant necrosis and poor differentiation (Fig. 2A).

IHC showed positive staining for SYN, CD56, vimentin, with Ki-67 >30%, and negative staining for CD99, WT1, EMA, and desmin. FISH showed negative for both *c-Myc* and *n-Myc* amplification (Fig. 2B).

IHC revealed positive staining of MMR markers, hMSH2 and hMLH1, in the nucleus region in normal kidney in this case. This was the same result as obtained from tissues of another neuroblastoma case without identified mutation (Fig. 2C), as well as other control tissues (data not shown). No significant decrease in hMSH2 and hMLH1 levels was found in this case.

3.3. Somatic mutations revealed by NGS

A total of 9666 somatic SNVs from 5148 genes were detected. The number of somatic SNV detected in different regions of the genes is shown in Table 2. Among the 3111 mutations in the exon-coding CDS region, 1469 mutations of missense, stoploss, and stopgain mutations that would cause change of amino acid sequences or the length of proteins. A total of 1171 genes were affected, and 1008 (85.9%) were mapped to 1386 distinct proteins in ConsensusPathDB. In pathway analysis, a total of 608 genes (53.4%) were present in at least one of 19 pathways identified. The 19 pathways enriched in mutated genes/proteins are listed in Table 3. NGS also revelaed 55 copy number variations (CNVs) and 140 insertion–deletion variations (INDELs) in this case.

Table 4 contains the druggable gene targets predicted by detected mutations. Potentially effective drugs in targeted therapy were anti-EGFR antibodies, and anthracyclines/related substances such as adriamycin. It was also suggested that the tumor cells could be sensitive to HMG-CoA and ACEI, which are nonrelevant to tumor chemotherapy.

Mutation of *MSH2* is shown in Table 5. A heterozygous mutation C23T from exon 1 of this gene was identified, leading to a mutation of T8 M in the protein level. The mutation rate was 6.3% (2/48) in this sample.

4. Discussion

Here we report a case of highly malignant neuroblastoma with diffused metastatic loci in the lung. Pathological examination

Table 1

The timeline of the reported case from initial diagnosis to death.

Age	Summaries from initial and follow-up visits	Diagnostic testing	Interventions
2 years and 8 months	The patient was a boy aged 2 years and 8 months when first admitted to the hospital for palpable left-side abdominal mass.	Needle biopsy and pathological examinations diagnosed the patient as neuroblastoma with poor differentiation. CT revealed multiple migration loci in the lung and pleural fluid, but no migration to the liver and the bone.	Five times of chemotherapy in 4 months by combination of vindesine+ifosfamide+etoposide and vindesine+theprubicine +carboplatin, topotecan, and gemcitabine were also used.
3 years and 1 month (before surgery)	The patient gained relapse following combined chemotherapy.	CT showed that after first session of chemotherapy, both the number and the size of the high-density loci in the lung were reduced.	Radical section of the tumor together with the left kidney and the left adrenal gland was performed.
3 years and 1 month (after surgery)	The patient developed severe bone marrow suppression following postsurgical chemotherapy for 4 times, with low white blood cell and platelet counts, and severe respiratory inflammation.	Pathological examinations confirmed neuroblastoma with poor differentiation and massive necrosis. Follow-up CT scans found no relapse of the original tumor in the adrenal gland, but multiple metastatic loci in both lungs, with new loci developed after the operation.	Eleven times of postsurgical chemotherapy protocols similar with the previous.
4 years and 6 months	The patient died.		

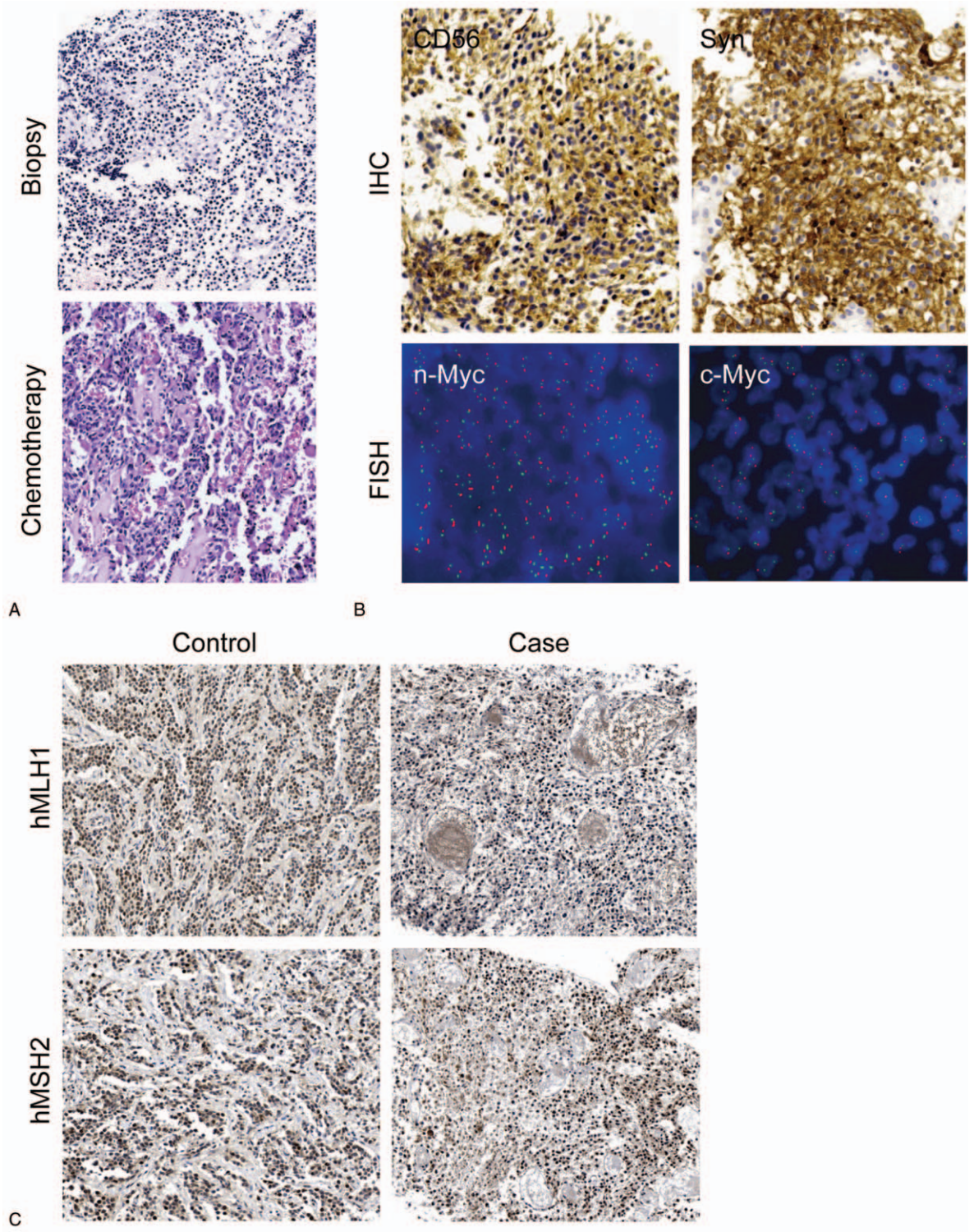

Figure 2. Expression of *Myc* gene and MMR proteins in the tumor tissues. (A) HE staining of tumor tissues obtained by needle biopsy and by surgery (200×). (B) IHC of CD56 and Syn, and FISH analysis of *c-Myc* and *n-Myc* of tumor tissue sectioned after chemotherapy (400×). (C) IHC of hMLH1 and hMSH2 in this case and a control neuroblastoma case without identified MMR mutation (200×).

revealed typical undifferentiated neuroblastoma cells. MDR of the metastatic tumors, as well as bone marrow suppression after chemotherapy, has made it an obstinate case in pediatric oncology. To study the genetic background of the tumor and to search for drug targets, NGS was performed to analyze the somatic mutations in the exon region. A substantially increased number of somatic mutations, especially SNVs, were identified. However, the underlying mechanism of the malignacy remained undefined. It is known that severe neuroblastoma cases are frequently associated with amplication of the *Myc* gene. Other

Table 2

The number of somatic SNV detected in different regions of the genome.

Type of mutation	Number
CDS	3111
synonymous_SNP	1612
missense_SNP	1451
stopgain	14
stoploss	3
unknown	31
Intronic	4780
UTR3	261
UTR5	171
Splicing	60
ncRNA_exonic	211
ncRNA_intronic	253
ncRNA_UTR3	10
ncRNA_UTR5	4
ncRNA_splicing	1
Upstream TSS	100
Downstream TTS	45
Intergenic	659
Total	9666

CDS = coding sequence, ncRNA = noncoding RNA, SNP = single-nucleotide polymorphism, TSS = transcription start site, TTS = transcription termination site, UTR = untranslated region.

driver genes including *p53* and *ALK* are also frequently involved. However, in this case, even with a powerful tool of NGS, no SNV, INDEL, or CNV mutations of the above key driver genes have been found. On the other hand, a total of 9666 somatic SNVs from 5148 genes were detected, and pathway analysis implies that many cellular functions could be impaired, such as cellular matrix and immune response. The relationship between the many somatic SNVs and the dysregulation of cellular pathways remains unclear.

Defects in the DNA repair system can cause genome instability and increased mutation rate. One important mechanism is the MMR system. Germ-line mutations of MMR-related genes lead to the Lynch syndrome, previously called HNPCC. However, in this case, the genes of all MMR components do not carry mutations except for *MSH2* that carried a heterozygous missense SNV mutation. Based on a recent study of functional screening to identify pathogenic *MSH2* mutation, the T8M mutation was proved to be nonpathogenic.[17] Further IHC analysis did not produce evidence of MMR deficiency in the protein level.

Table 4

Therapeutic targets predicted by analysis of mutated genes.

Gene(s)	Drug target(s)
ROS1	Anti-EGFR antibodies
FCGR3A	Cetuximab (anti-EGFR antibody)
UGT1A10, SLC28A3	Anthracyclines and related substances (Adriamycin)
SLCO1B1	HMG-CoA reductase inhibitors
NR3C2	Angiotension converting enzyme inhibitors (ACEI)

Although NGS can be a powerful tool to guide personalized precision treatment, at current stage, even without consideration of the relatively high cost, its application in the clinic still has its limits. First, the procedure to obtain representative tumor tissue has intrinsic difficulty because tumors are highly heterogeneous. Sites like lung metastatic loci are not readily accessible for biopsy. In this case, some lung migration sites were responsive to treatment, whereas others manifested different response. Theoretically, it would be informative to compare the genetics of different loci, but is difficult to practice. Second, the number of druggable target molecules is limited. In this case, drug target analysis based on NGS data suggested that the tumor might be sensitive to anti-EGFR antibodies and adriamycin. Although anti-EGFR antibodies are potentially effective, they are not readily available in the clinic of pediatric oncology in China and in many developing countries. Furthermore, there are many potential targets without effective compounds. It is somewhat perplexing that in our clinical protocol, vindesine, an analogue of adriamycin predicted as an effective treatment option, did not result in improved clinical outcome, suggesting the current data

Table 3

The pathways enriched in mutated genes/proteins analyzed by ConsensusPathDB.

Pathway name	Set size	Candidates contained	*P*	*q*	Pathway source
Extracellular matrix organization	264	33 (12.5%)	5.71e–06	0.0063	Reactome
Thyroid hormone synthesis	9	5 (55.6%)	4.88e–05	0.0216	SMPDB
Antigen processing and presentation—Homo sapiens	77	14 (18.2%)	5.85e–05	0.0216	KEGG
ECM-receptor interaction—Homo sapiens	87	14 (16.1%)	.00023	0.0631	KEGG
Immunoregulatory interactions between a Lymphoid and a non-Lymphoid cell	146	18 (12.6%)	.00072	0.134	Reactome
Olfactory signaling pathway	427	36 (8.5%)	.00528	0.411	Reactome KEGG
Pregnane X receptor pathway	33	7 (21.2%)	.00167	0.231	Wikipath
ABC transporters—Homo sapiens	44	8 (18.2%)	.00225	0.277	KEGG
Interaction between L1 and Ankyrins	29	6 (20.7%)	.00407	0.386	Reactome
Cell adhesion molecules (CAMs)—Homo sapiens)	142	16 (11.3%)	.00437	0.386	KEGG
Irinotecan pathway	14	4 (28.6%)	.00557	0.411	PharmGKB Wikipath
Graft vs host disease—Homo sapiens	41	7 (17.1%)	.00603	0.417	KEGG
Constitutive androstane receptor pathway	32	6 (18.8%)	.00676	0.423	Wikipath
Collagen formation	87	11 (12.6%)	.00724	0.423	Reactome
CDC6 association with the ORC:origin complex	8	3 (37.5%)	.00727	0.423	Reactome
Anchoring of the basal body to the plasma membrane	90	11 (12.4%)	.00857	0.446	Reactome
Assembly of collagen fibrils and other multimeric structures	44	7 (15.9%)	.00893	0.446	Reactome
Cobalamin (Cbl, vitamin B12) transport and metabolism	16	4 (25.0%)	.00929	0.446	Reactome
Saturated fatty acids beta-oxidation	25	5 (20.0%)	.00998	0.446	EHMN

Table 5

Characteristics of *MSH2* mutations identified.

GeneName	*MSH2*
CHROM	2
POS	47630353
REF	C
ALT	T
Func	exonic
ExonicFunc	missense SNV
AAChange	MSH2:NM_000251:exon1:c.C23T:p.T8M
cytoBand	2p21
FORMAT	GT:AD:BQ:DP:FA:SS
CX05N	0:48,0:48:0.00:0
CX05T	0/1:45,3:42:48:0.063:2

AD = allelic depths for the ref and alt alleles in the order listed, BQ = average base quality for reads supporting alleles, DP = approximate read depth (reads with MQ = 255 or with bad mates are filtered), FA = allele fraction of the alternate allele with regard to reference, GT = genotype, homozygous=0/0 or 1/1, heterozygous=0/1, SS = variant status relative to nonadjacent normal, 0 = wild type, 1 = germline, 2 = somatic, 3 = LOH, 4 = posttranscriptional modification, 5 = unknown.

interpretation tools could be inadequate. The last but not the least, our knowledge toward the genetics background of neuroblastoma is still very limited. The case reported is an example of pronounced somatic mutations but without identified driver gene and therapeutic target. Deeper understanding of the oncogenetics, as well as optimization of analytical tools, must be achieved before NGS data can provide more diagnostic and therapeutic insight in the clinic.

Acknowledgments

The authors thank professor Jian Chen from Institute of Translational Medicine, Zhejiang University, for his help with the analysis of DNA MMR.

References

[1] Brodeur GM, Pritchard J, Berthold F, et al. Revisions of the international criteria for neuroblastoma diagnosis, staging, and response to treatment. J Clin Oncol 1993;11:1466–77.

[2] Dubois SG, London WB, Zhang Y, et al. Lung metastases in neuroblastoma at initial diagnosis: a report from the International Neuroblastoma Risk Group (INRG) project. Pediatr Blood Cancer 2008;51:589–92.

[3] Theruvath J, Russo A, Kron B, et al. Next-generation sequencing reveals germline mutations in an infant with synchronous occurrence of nephro- and neuroblastoma. Pediatr Hematol Oncol 2016;33:264–75.

[4] Sanmartin E, Munoz L, Piqueras M, et al. Deletion of 11q in Neuroblastomas Drives Sensitivity to PARP Inhibition. Clin Cancer Res 2017;23:1–3.

[5] Lasorsa VA, Formicola D, Pignataro P, et al. Exome and deep sequencing of clinically aggressive neuroblastoma reveal somatic mutations that affect key pathways involved in cancer progression. Oncotarget 2016;7:21840–52.

[6] Pugh TJ, Morozova O, Attiyeh EF, et al. The genetic landscape of high-risk neuroblastoma. Nat Genet 2013;45:279–84.

[7] Eleveld TF, Oldridge DA, Bernard V, et al. Relapsed neuroblastomas show frequent RAS-MAPK pathway mutations. Nat Genet 2015;47:864–71.

[8] Lee YH, Kim JH, Song GG. Genome-wide pathway analysis in neuroblastoma. Tumour Biol 2014;35:3471–85.

[9] Schramm A, Koster J, Assenov Y, et al. Mutational dynamics between primary and relapse neuroblastomas. Nat Genet 2015;47:872–7.

[10] Fishel R. Mismatch repair. J Biol Chem 2015;290:26395–403.

[11] Wimmer K, Rosenbaum T, Messiaen L. Connections between constitutional mismatch repair deficiency syndrome and neurofibromatosis type 1. Clin Genet 2016;91:507–19.

[12] Kolodner RD, Hall NR, Lipford J, et al. Human mismatch repair genes and their association with hereditary non-polyposis colon cancer. Cold Spring Harb Symp Quant Biol 1994;59:331–8.

[13] Ponti G, Castellsague E, Ruini C, et al. Mismatch repair genes founder mutations and cancer susceptibility in Lynch syndrome. Clin Genet 2015;87:507–16.

[14] Idikio HA. Expression of DNA mismatch repair proteins hMSH2 and hMLH1 and the cyclin G1 inhibitor, p21 (waf1/cip1) in pediatric tumors: correlation with response to therapy. Oncol Rep 2001;8:965–71.

[15] Collins SL, Herve R, Keevil CW, et al. Down-regulation of DNA mismatch repair enhances initiation and growth of neuroblastoma and brain tumour multicellular spheroids. PLoS One 2011;6:e28123.

[16] Ambros IM, Benard J, Boavida M, et al. Quality assessment of genetic markers used for therapy stratification. J Clin Oncol 2003;21:2077–84.

[17] Houlleberghs H, Dekker M, Lantermans H, et al. Oligonucleotide-directed mutagenesis screen to identify pathogenic Lynch syndrome-associated MSH2 DNA mismatch repair gene variants. Proc Natl Acad Sci USA 2016;113:4128–33.